Precision Engineering 42 (2015) 276–282

Contents lists available at ScienceDirect

Precision Engineering

journal homepage: www.elsevier.com/locate/precision

Development of high-precision micro-roundness measuring machine using a high-sensitivity and compact multi-beam angle sensor

Meiyun Chen[a], Satoru Takahashi[b], Kiyoshi Takamasu[a,*]

[a] Faculty of Engineering, Department of Precision Engineering, The University of Tokyo, 7-3-1 Hongo, Bunkyo-ku, Tokyo 113-8656, Japan
[b] Research Center for Advanced Science and Technology, The University of Tokyo, 4-6-1 Komaba, Meguro-ku, Tokyo 153-8904, Japan

ARTICLE INFO

Article history:
Received 19 January 2015
Accepted 15 May 2015
Available online 2 June 2015

Keywords:
Micro-RMM
Multi-beam angle sensor
Roundness
Autocollimator
Stage-independence

ABSTRACT

With recent development in advanced manufacturing, demand for nanometric accuracy in dimensional metrology has increased dramatically. To satisfy these requirements, we propose a high-accuracy micro-roundness measuring machine (micro-RMM) using a multi-beam angle sensor (MBAS). The micro-RMM includes three main parts: the MBAS, a rotary unit, and a bearing system. The MBAS has been designed and established in order to improve motion accuracy of the micro-RMM. The dimensions of the MBAS are 125(L) mm × 130(W) mm × 90(H) mm. Compared with other methods, an MBAS is less susceptible to spindle error (stage-independence) when detecting angles, can maintain high sensitivity with miniaturized size, and can be used conveniently at the factory level. The optical probe, reported in this paper, is based on the principle of an autocollimator, and the stability is improved when using the MBAS. Unlike multi-probe methods, the micro-RMM is constructed to realize roundness measurement by using only one probe, which is less susceptible to instrumental errors. Experimental results confirming the feasibility of the multi-beam angle sensor for roundness measurement are also presented.

© 2015 Elsevier Inc. All rights reserved.

1. Introduction

In recent years, there has been a growing demand for high-accuracy surface roundness measurement techniques and for simple instruments that can be used conveniently in situ, including in fields such as optical metrology, semiconductors, and space satellites [1–3].

To measure roundness errors of cylindrical workpieces and spindle errors of machine tools in on-machine conditions, it is important to distinguish between roundness error and spindle error. There are two methods of distinguishing these errors: the multi-orientation method and the multi-probe method [4–7].

The multi-orientation method can differentiate the spindle error and the roundness error effectively if the spindle error has good repeatability. Compared with multi-orientation methods, multi-probe methods are more suitable for on-machine measurements because it does not depend on the repeatability of the spindle error [8–10].

Reversal methods can be used to eliminate the systematic errors of a spindle; however, they are very time consuming and still demand good repeatability of spindle motion. This has led us to the solution of using the measured object itself as a reference by employing the three-point method [11–13]. However, using numerous sensors makes it difficult to attach or remove the measured object, and it is not easy to adjust the direction of the sensor's radius.

Several techniques have been proposed and developed for measuring roundness precisely. Each of these methods comes with its own advantages, disadvantages, and limitations [14–18]. This paper analyzes existing techniques and proposes a new technology called multi-beam angle sensor (MBAS) for measuring roundness [19].

From an engineering point of view, the most useful type of surface metrology instrument would probably have an accurate axis of rotation and accurate Cartesian and radial movements; furthermore, it would measure according to a cylindrical frame of reference. However, the disadvantages are that they it can only be used under laboratory conditions, and to get better results, it is necessary to match the co-ordinate system of the measuring instrument to that of the component [20].

In this study, an MBAS based on an autocollimator is proposed for roundness measurement. Compared to other technologies, the micro-RMM uses just one sensor that is less susceptible to instrumental errors when detecting angles, the dimensions of the MBAS are 125(L) mm × 130(W) mm × 90(H) mm which can be used conveniently at the factory level [21]. In addition, a simple optical-path

* Corresponding author. Tel.: +81 03 5841 6472; fax: +81 03 5841 6472.
E-mail address: chenmeiyun@nanolab.t.u-tokyo.ac.jp (K. Takamasu).

http://dx.doi.org/10.1016/j.precisioneng.2015.05.009
0141-6359/© 2015 Elsevier Inc. All rights reserved.

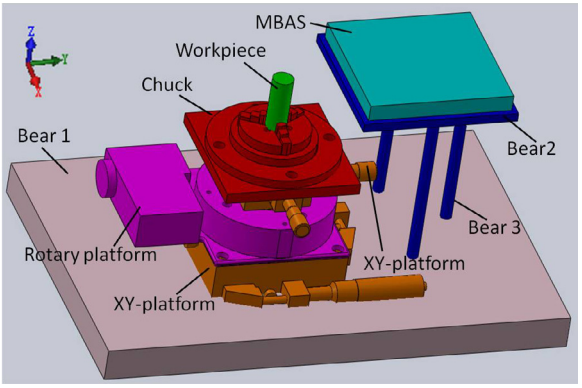

Fig. 1. Schematic of the micro-RMM: an MBAS, a rotary unit, and a bearing system.

design enables the proposed setup to be insensitive to environmental vibration.

2. Micro-RMM configuration

The micro-RMM configuration includes three main parts: an MBAS, a rotary unit, and a bearing system. The MBAS is based on a multi-autocollimator system using a microlens array. It works by projecting an image onto a beam splitter, and measuring the deflection of the returned image against a scale. The reflected angles at several points on the cylindrical workpiece can be measured by a sensor, and the curvature of the workpiece can be calculated by the difference between the two reflected angles. Therefore, the micro-RMM can realize roundness measurement by using the curvature, which is less susceptible to instrumental errors.

Using the MBAS, we designed the experimental system shown in Fig. 1. A cylindrical workpiece is mounted on a chuck, and a rotary platform is mounted between two *XY*-platforms. For roundness measurement, the cylindrical workpiece is rotated by the rotary platform. The axis of rotation of the workpiece spindle is represented by the *Z*-axis. In any roundness measuring instrument, the spindle of a rotary stage is the most important component in its assembly. Here, when the workpiece is assembled, it is necessary to align the *Z*-axis and the axis of the rotary platform to be collinear. The alignment is performed by adjusting the positions of the two *XY*-platforms. Along with the upper *XY*-platform, which is used to achieve minimal spindle error between the workpiece and rotary stage, the lower one is used to approach an almost perfect position between the MBAS and rotary stage.

Fig. 2 illustrates the construction of the MBAS. A laser beam passes through a pinhole and is collimated by a collimator lens. The beam is then bent by a beam splitter and projected through

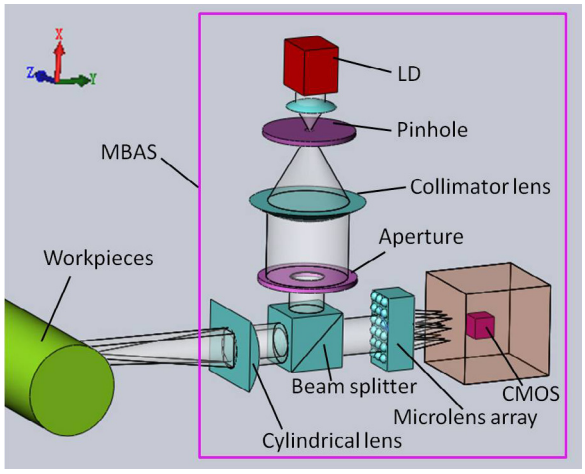

Fig. 2. Construction of the MBAS: the multi-beam angle sensor is based on a multi-autocollimator system using a microlens array.

a cylindrical lens to the workpiece surface. The cylindrical lens is employed in the sensor for removing the influence of the curvature of the cylinder's surface. The reflected beam from the workpiece surface passes through the beam splitter and is focused on a microlens array, which divides the beams into several beams. The resulting pattern is observed and recorded by a CMOS camera mounted along the vertical axis. The image can be observed on a TV monitor. Further processing of the pattern is performed using a PC.

3. Principle of the MBAS

3.1. Calculating the angle difference Δc

To measure roundness errors of a cylindrical workpiece, it is important to obtain the relationship between the radius and the curvature. Fig. 3 illustrates the changing radius of curvature of the workpiece. The red and blue lines delineate a small radius with high curvature and a large radius with low curvature, respectively, f_1 and f_2 are the focal distances of the cylindrical lens and microlens array, respectively, R and r is the radius of curvature of the large radius and small radius, respectively, and x_0 and x_1 are the distance between points A and B, A_1 and B_1 in Fig. 3 of the low curvature and high curvature images, respectively.

Fig. 4 shows the principle of an angle difference measured by the MBAS. Let A and B be representative points of the workpiece. When the radius of curvature changes from R to r, the distance between two points change from x_0 to x_1.

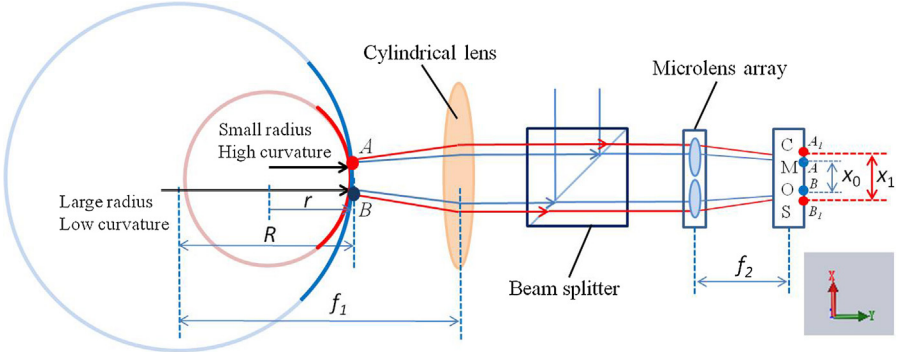

Fig. 3. Radius of curvature comparison: the red and blue lines delineate a small radius with high curvature and a large radius with low curvature, respectively.

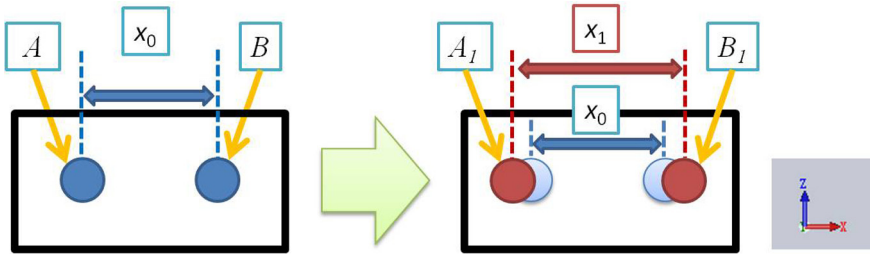

Fig. 4. Calculating the angle difference: from intensity distribution of the center of gravity.

Fig. 5 illustrates the change in angle of a reflected ray when the curvature changes from R to r. The value R–r and t is small compared to R. Thus, it is easily understood that the change in angle of a reflected ray Δc on the surface can be described by the following equation:

$$\Delta c = \frac{1}{r} - \frac{1}{R} = \frac{c_r}{Rt} \tag{1}$$

When the angle of a reflected ray c_r from the workpiece surface passes through the cylindrical lens and microlens array, the output image on the CMOS is presented in Fig. 3. Here, the relationship between the change in the distance of two points Δx and the change in angle of a reflected ray c_r can be calculated as follows:

$$\Delta x = \frac{c_r R f_2}{f_1} \tag{2}$$

Clearly, from Eqs. (1) and (2), the change in angle of a reflected ray Δc can be expressed as

$$\Delta c = \frac{\Delta x f_1}{f_2 R t} = \frac{(x_1 - x_0) f_1}{f_2 R^2 t} \tag{3}$$

3.2. Reducing rotary stage susceptibility

Fig. 6 shows the path of a reflected beam from the surface of a cylindrical workpiece. An optical probe is used to scan the cylindrical workpiece while the workpiece is rotating. Assuming that the center of the cylinder (eccentricity) is at O_1 (o_x, o_y) and the cylinder radius is R and using the MBAS, we can obtain the two measured angles c_a and c_b.

Assuming that the center of the cylinder is O_1 (o_x, o_y), W is a representative point on the workpiece, and the cylinder radius is R, we can obtain the distance of the projected beam b_a by the relationship between the points O, O_1 and W. The distance b_a is then given by

$$(b_a \cos t - o_x)^2 + \left(b_a \sin t - o_y\right)^2 = R^2 \tag{4}$$

$$b_a = o_x \cos t + o_y \sin t + \sqrt{\left(o_x \cos t + o_y \sin t\right)^2 + \left(R^2 - o_x^2 - o_y^2\right)} \tag{5}$$

Through the model of triangle $\Delta O O_1 W$, the cosine theorem is used to evaluate the angle c_a, where $2c_a$ is the reflection angle. The angle c_a is given by

$$o_x^2 + o_y^2 = R^2 + b_a^2 - 2R b_a \cos c_a \tag{6}$$

$$\cos c_a = \frac{R^2 + b_a^2 - o_x^2 - o_y^2}{2R b_a} = \frac{\sqrt{R^2 - o_x^2 - o_y^2 + \left(o_x \cos t + o_y \sin t\right)^2}}{R} \tag{7}$$

Furthermore, we can approximate c_a and c_b as follows:

$$\cos c_a \approx 1 + \frac{-o_x^2 - o_y^2 + \left(o_x \cos t + o_y \sin t\right)^2}{2R^2} \approx 1 - \frac{c_a^2}{2} \tag{8}$$

$$c_a \approx \frac{o_y \cos t - o_x \sin t}{R} \tag{9}$$

$$c_b \approx \frac{o_y \cos t + o_x \sin t}{R} \tag{10}$$

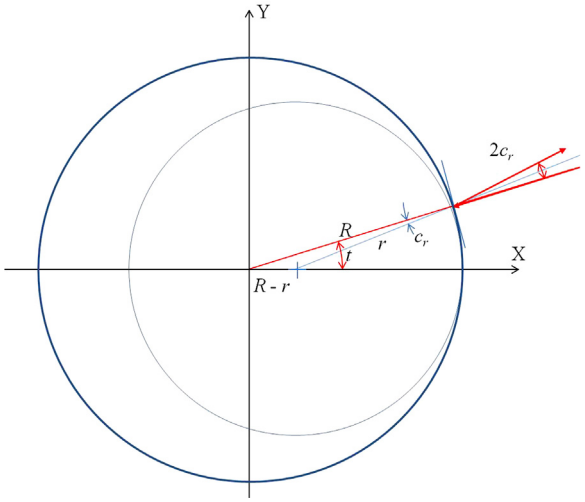

Fig. 5. The change in angle of a reflected ray when the curvature changes from R to r.

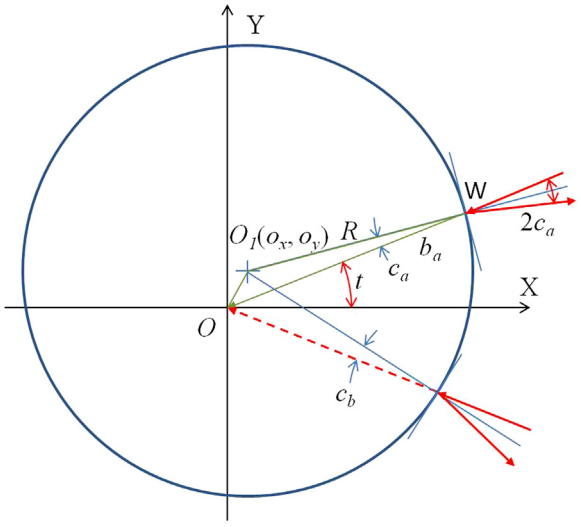

Fig. 6. Relation between eccentricity and reflected beam.

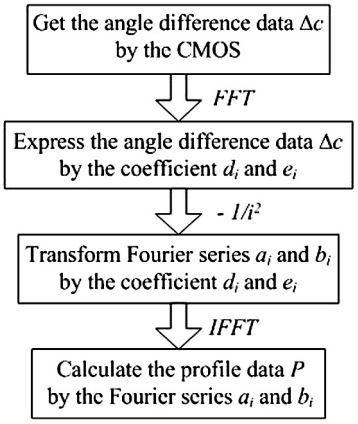

Fig. 7. Algorithm flowchart of the measurement: from angle difference Δc to profile data P use Fourier series.

From Eqs. (9) and (10), the transform of Δc ($=c_a - c_b$), which is the combination that eliminates o_y, is calculated by a simple arithmetic:

$$c_a - c_b \approx \frac{-2o_x \sin t}{R} \tag{11}$$

The value of o_x is small compared to R. Additionally, the influence of the term ($o_x \sin t$) is small. More will be said on this topic in Section 4, the experimental results in Section 4.2 will confirm that the angle difference value Δc is found to be small enough when comparing with random angle error.

Here, the curvature is the angle difference in the small area, and the curvature of the workpiece can be calculated by the angular difference of two reflected beams. Therefore, the micro-RMM can realize roundness measurement by using the curvature, which is less susceptible to instrumental errors.

3.3. Calculating the profile P

Fig. 7 shows the algorithm flowchart of the measurement. The profile data P of workpiece in position t can be expressed as a Fourier series, given by

$$P(t_j) = a_0 + \sum_{i=1}^{n} \left(a_i \cos t_j i + b_i \sin t_j i\right)$$
$$t_j = \frac{2\pi(j-1)}{m} \quad (j = 1, 2, \ldots, m) \tag{12}$$

where a_i and b_i are the Fourier series coefficients, n the maximum iterations of the Fourier series, and m the number of sample points. Here, the angle difference Δc can be measured by the sensor, and can also be expressed as the second order differential of the profile data P, given by

$$\Delta c\left(t_j\right) = P''\left(t_j\right) = -\sum_{i=1}^{n} i^2 \left(a_i \cos t_j i + b_i \sin t_j i\right) \tag{13}$$

Then, using a Fourier transformation, we can also transform the angle difference Δc to coefficients d_i and e_i, given by the following equation:

$$c_j = \sum_{i=1}^{n} \left(d_i \cos t_j i + e_i \sin t_j i\right) = P''\left(t_j\right) \tag{14}$$

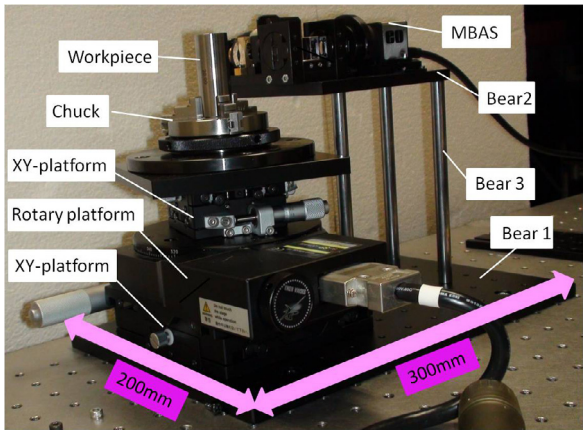

Fig. 8. Micro roundness measuring machine for noncontact roundness measurement: the main setup of the pre-experiment consisted of the MBAS, two *XY*-platforms, a rotary platform, a chuck, and a bearing system.

We note that the relationship between the Fourier series (a_i and b_i) and coefficients (d_i and e_i) can be denoted as

$$a_i = -\frac{d_i}{i^2}, \; b_i = -\frac{e_i}{i^2} \tag{15}$$

Consequently, the profile data P can be denoted as a Fourier series by using an inverse Fourier transform.

The characteristics of the algorithm chart can be estimated by its transfer function, which defines the relationship between the angle difference value Δc and profile data P.

4. Pre-experiment and simulation

4.1. Configuration of the pre-experiment

The pre-experimental arrangement is shown in Fig. 8. In the pre-experiment, the MBAS is based on a multi-autocollimator system using a microlens array. Table 1 shows the specifications of the devices in Fig. 8. The main setup of the pre-experiment consisted of the MBAS, two *XY*-platforms, a rotary platform, a chuck, and a bearing system. We used a stage controller to move the rotary platform by using the Labview program in our PC to receive the output signals from the MBAS in each measuring position.

Fig. 9 illustrates the construction of the MBAS. A laser beam from an LD (laser diode) of 650 nm wavelength passes through a pinhole with a diameter of 400 μm and is collimated by the microlens. The beam is then bent by a beam splitter and projected through a cylindrical lens with a focal distance of 50 mm to the workpiece surface. The cylindrical lens is employed in the sensor for removing the influence of the curvature of the cylinder's surface. The reflected beam from the workpiece surface passes totally through the beam splitter and focuses it on the microlens array, which divides the

Table 1
Specifics of devices in micro-RMM (Fig.8).

Laser Diode	Output power: 35 mW (CW) Wavelength: 658 nm
Cylindrical lens	Focal distance: 50 mm (f_1)
Pinhole	Diameter: 400 μm
Aperture	Diameter: 4 mm
Microlens array	Focal distance: 46.7 mm (f_2)
	Pitch of the array: 500 μm
CMOS	Size: 5.6 mm × 4.2 mm
	Valid pixels: 2560 pixel × 1920 pixel
	Sensitive area: 2.2 μm × 2.2 μm

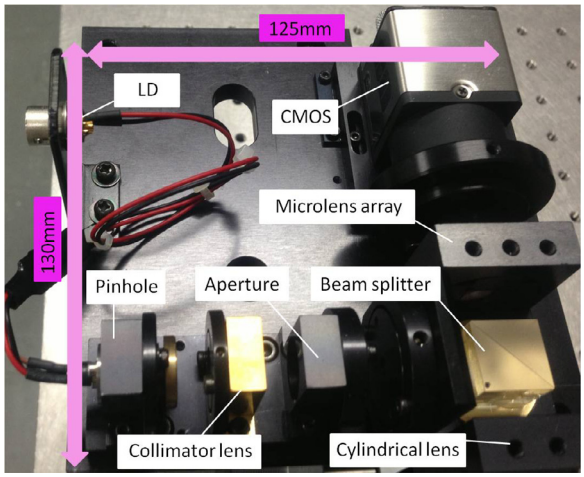

Fig. 9. Construction of the multi-beam angle sensor: the MBAS is based on a multi-autocollimator system using a microlens array.

beams into several beams. The resulting pattern is observed and recorded by a CMOS camera mounted along the vertical axis.

Fig. 10(a) shows an example of one output signal from the CMOS. The scatter plot presents eight lines by eight columns. We choose the points in number four line to calculate the data. In Fig. 10(b) you can see the intensity distribution in the whole and in a spot. By using the intensity distribution, the angle difference data can be calculated. Then, using centroid, we can also estimate the resolution of sensor is about 0.05 μrad.

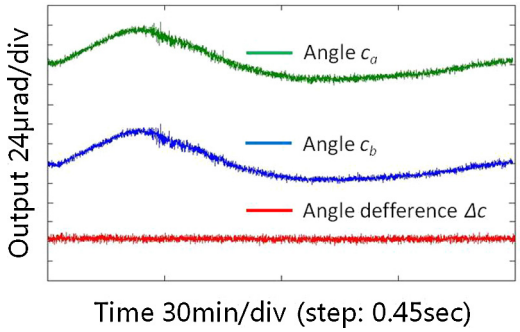

Fig. 11. Stability of multi-beam angle sensor: we measured the stability of angle and angle difference for 2 h.

4.2. Stability of the MBAS

In order to verify the standard deviation of the measurement taken by MBAS in the real environment, we measured the stability of angle and angle difference for 2 h. Fig. 11 shows the results of the angle at point A and point B. In the stability test of the MBAS, the output signals were sampled without rotating the cylinder; therefore, in the pre-experiment, the stability of the MBAS corresponds to the standard deviation of the autocollimator.

The experimental setup is mounted on a table in the basement. In Fig. 11, because the test time was long and the influence of the thermal drift was large. The standard deviation of the angle data at point A was 18.36 μrad. However, the stability of angle difference output was 2.35 μrad. We note that the fluctuation of stability of

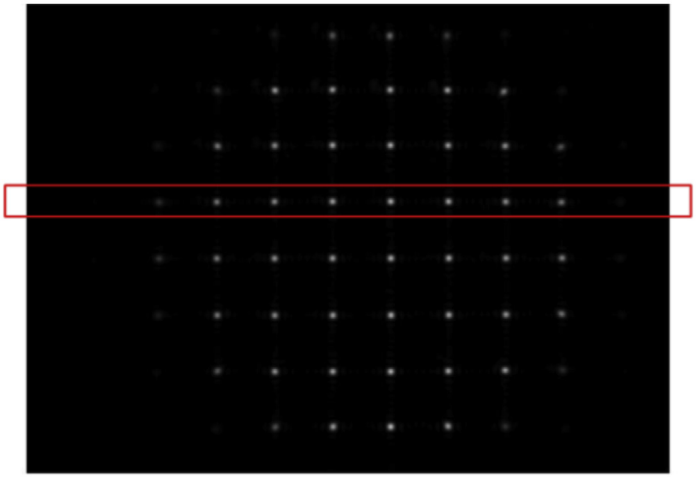

(a) Image from the CMOS

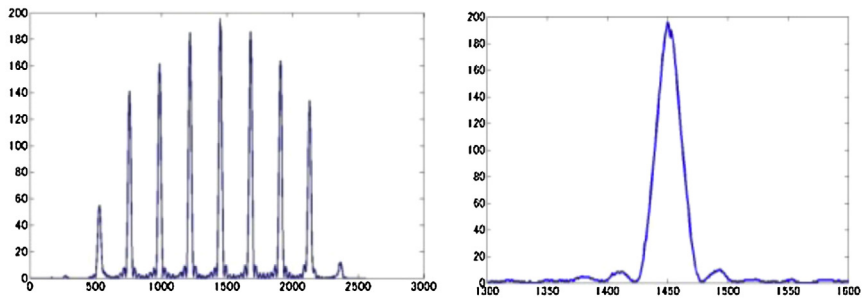

(b) Intensity distribution: calculate the angle difference data from intensity distribution

Fig. 10. Image from the CMOS.

Table 2
Experimental conditions.

Parameters	Values
Diameter of cylinder	20 mm
Sample points	360
Rotation angle of one point	1 degree
Measuring time	14 min

angle difference was slight because it eliminated influence of thermal drift. Here, only the characteristics of the differential output to measure the roundness will be investigated.

Assuming that the value of o_x is 1 μm, t is 2000 as, and R is 10 mm. From Eq. (11), we can calculate the $(c_a - c_b)$ to be 2 μrad in the experimental condition. The experimental results also confirmed that the angle difference value Δc reached the same level with random angle error.

From the stability testing results, we note that a simple optical-path design enables the proposed setup to be insensitive to environmental vibration.

4.3. Pre-experiment results

Table 2 shows the experimental conditions. Fig. 12 shows the angle data c_a and c_b by MBAS system. The horizontal axis is the rotation angle and the vertical axis is the angle data.

Measured results presented in Fig. 13 shows the roundness on average of four times was 2.26 μm with standard deviation 0.027 μm.

To evaluate the developed methodology based on the MBAS method on real datasets, an experiment was developed using conventional high-precision machines (KOSAKA EC1550) for roundness assessment. Here, the roundness measurement accuracy of EC1550 is 0.02 μm. Fig. 14 shows the roundness measurement of two separate measurement methods. The roundness for the MBAS method and radius method are 2.26 μm and 2.16 μm, respectively. The roundness test with MBAS system was performed in a circumstance without any temperature control or vibration isolation. Therefore, the influence of circumstance may be one reason to the differential output of two methods.

The pre-experiment results confirm the feasibility of the MBAS for roundness measurement. In the future, we still need to analyze factors influencing measurement accuracy and find measures adopted for evaluating and calibrating the MBAS.

4.4. Simulation of sensitivity error of the MBAS

To confirm the effectiveness of the sensitivity error of the sensor, numerical simulations were performed. Table 3 shows the simulation conditions. Supposing a random angle error of 2.4 μrad, where roundness is 2.2 μm, Fig. 15 shows a simulation example with

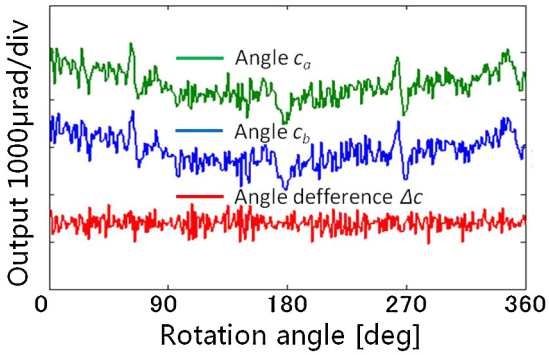

Fig. 12. Measured angle data at points A and B and angle difference data.

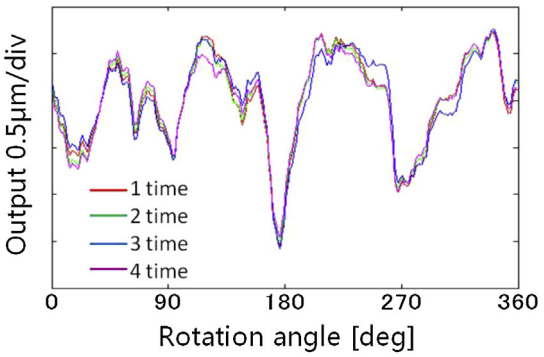

(a) Profile data (four trials)

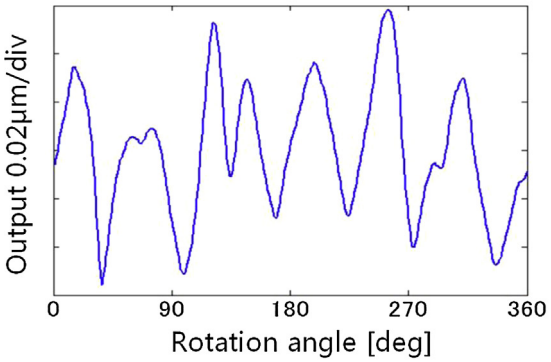

(b) Repeatability (STD)

Fig. 13. Profile data and repeatability for a cylinder measured by the MBAS.

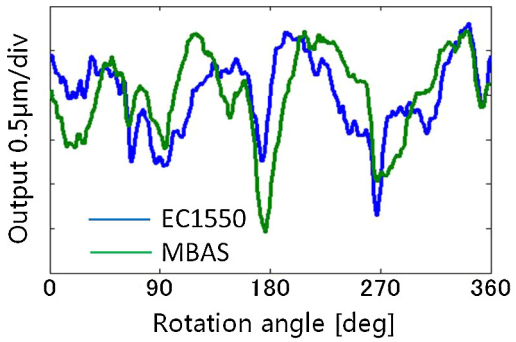

Fig. 14. Comparison with the radius method.

similar conditions as those of the pre-experiment. During 10 simulations, we obtained roundness measurements with repeatability around 0.03 μm (see Fig. 15). Despite the simplicity of the proposed method, the simulated results agree well with experimental data.

Under similar experimental conditions, the standard deviation of repeatability is proportional to the random value. The simulation result implies that this system can measure roundness with repeatability under 10 nm if the random angle error is less than

Table 3
Simulation conditions.

Parameters	Values
Diameter of cylinder	20 mm
Sample points	360
Roundness	2.2 μm
Random angle error	2.4 μrad

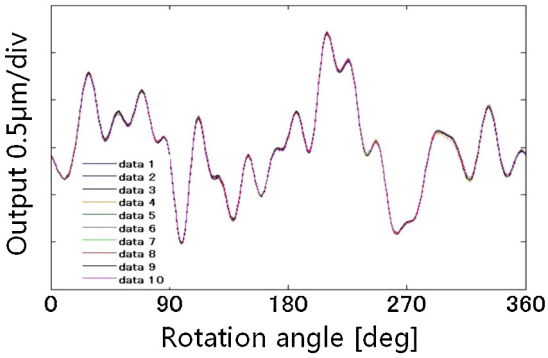

Fig. 15. Sensitivity of the sensor (10 times).

0.8 μrad. Therefore, a further improvement of measurement accuracy could be achieved by reducing the random error of MBAS.

5. Conclusions

The results of this paper are summarized as follows:

(1) A high accuracy micro roundness measuring machine (micro-RMM) for accurately measurement the roundness profiles has been proposed in this paper. The schematic of the micro-RMM includes three main parts: a multi-beam angle sensor (MBAS), a rotary unit, and a bearing system. The MBAS has been incorporated in order to improve the motion accuracy of the micro-RMM. Compared with other methods, the MBAS is less susceptible to instrumental errors for angle detection, can maintain high sensitivity with a miniaturized size, and can be used conveniently at the factory level.
(2) A measurement system for roundness measurement using the MBAS has been constructed. The resolution of the MBAS is 0.05 μrad. The optical probe is based on the principle of an autocollimator and has a stability of 2.35 μrad. The roundness in the MBAS method and radius method are 2.26 μm and 2.16 μm, respectively. It can be seen that the standard deviation is approximately 0.17 μm. Experimental results confirm feasibility of the MBAS for roundness measurement are also presented.
(3) To confirm the effectiveness of the sensitivity error of the sensor, numerical simulations were performed with conditions similar to those of the experiment. Despite the simplicity of the proposed method, the simulated results agree well with experimental data. In a similar condition of the experiment, the standard deviation of repeatability is proportional to the random angle error. The simulation result implies that the proposed system can measure roundness with repeatability under 10 nm if stability of the angle difference value is less than 0.8 μrad.

As mentioned previously, the scatter plot in CMOS presents eight lines by eight columns. We use one line spots to measure the roundness. In the future, our instrument will measure not only roundness, but also axial form or vertical straightness, dimensional uniformity or parallelism by using the spots in axial direction.

We also plan to calibrate the autocollimator by analyzing factors influencing measurement accuracy or by finding measures adopted for high-speed measurement. A new experiment has been designed, which is planned to be conducted in the near future in order to implement the improvements.

References

[1] Chetwynd DG, Siddall GJ. Improving the accuracy of roundness measurement. J Phys E: Sci Instrum 1976;9(7):537–44.
[2] Whitehouse DJ. Some theoretical aspects of error separation techniques in surface metrology. J Phys E: Sci Instrum 1976;9:531–6.
[3] Shimizu Y, Goto S, Lee JC, Ito S, Gao W, Adachi S, et al. Fabrication of large-size SiC mirror with precision aspheric profile for artificial satellite. Precis Eng 2013;37:640–9.
[4] Vissiere A, Nouira H, Damak M, Gibaru O, David JM. A newly conceived cylinder measuring machine and methods that eliminate the spindle errors. Meas Sci Technol 2012;23(9):094015.
[5] Bernstein J, Weckenmann A. Measurement uncertainty evaluation of optical multi-sensor-measurements. Measurement 2012;45:2309–20.
[6] Mekid S, Vacharanukul K. In-process out-of-roundness measurement probe for turned workpieces. Measurement 2011;44:762–6.
[7] Gao W, Kiyono S. On-machine roundness measurement of cylindrical workpieces by the combined three-point method. Measurement 1997;21:147–56.
[8] Gleason E, Schwenket H. A spindleless instrument for the roundness measurement of precision spheres. Precis Eng 1998;22:37–42.
[9] Marsh E, Couey J, Vallance R. Roundness measurement of spherical artifacts at arbitrary latitude. Precis Eng 2006;30:353–6.
[10] Gao W, Huang PS, Yamada T, Kiyono S. A compact and sensitive two-dimensional angle probe for flatness measurement of large silicon wafers. Precis Eng 2002;26:396–404.
[11] Teimel A. Technology and applications of grating interferometers in high-precision measurement. Precis Eng 1992;14:147–54.
[12] Whitehouse DJ. Surface metrology. Meas Sci Technol 1997;8:955–72.
[13] Muralikrishnan B, Venkatachalam S, Raja J, Malburg M. A note on the three-point method for roundness measurement. Precis Eng 2005;29:257–60.
[14] Horikawa O, Maruyama N, Shimada M. A low cost, high accuracy roundness measuring system. Precis Eng 2001;25:200–5.
[15] Gao W, Tano M, Sato S, Kiyono S. On-machine measurement of a cylindrical surface with sinusoidal micro-structures by an optical slope sensor. Precis Eng 2006;30:274–9.
[16] Estler WT, Evans CJ, Shao LZ. Uncertainty estimation for multiposition form error metrology. Precis Eng 1997;21:72–82.
[17] Zeng L, Matsumoto H, Kawachi K. Multi-point dynamic displacement probe that uses a self-focusing microlens array. Opt Eng 1997;36:1361–6.
[18] Horikawa O, Sato K, Shimokohbe A. Roundness and absolute radial motion accuracy measurement by an improved reversal method. J Jpn Soc Precis Eng 1991;57:2231–6.
[19] Ueda S, Chen M, Takahashi S, Takamasu K. Roundness measurement of a cylindrical surface by a multi-beam angle sensor (1st report: Measurement method and verification scheme). In: 2014 JSPE spring conference. 2014.
[20] Smith GT. Industrial metrology: surfaces and roundness. London: Springer; 1993.
[21] Chen M, Ueda S, Miyazaki G, Takahashi S, Takamasu K. Roundness measurement of a cylindrical surface by a multi-beam angle sensor (2nd report: experimental verification and calibration of multi-beam angle sensor). In: 2014 JSPE autumn conference. 2014.